

Integrated lithium niobate intensity modulator on a silicon handle with slow-wave electrodes

SEAN NELAN^{1,2*}, ANDREW MERCANTE², SHOUYUAN SHI^{1,2}, PENG YAO², ELIEZER SHAHID², BENJAMIN SHOPP², AND DENNIS W. PRATHER^{1,2}

¹School of Electrical and Computer Engineering, University of Delaware, Newark, Delaware 19716, USA

²Phase Sensitive Innovations, Newark, Delaware 19713, USA

*Corresponding author: snelan@udel.edu

Compiled July 8, 2022

Segmented, or slow-wave electrodes have emerged as an index-matching solution to improve bandwidth of traveling-wave Mach Zehnder and phase modulators on the thin-film lithium niobate on insulator platform. However, these devices require the use of a quartz handle or substrate removal, adding cost and additional processing. In this work, a high-speed dual-output electro-optic intensity modulator in the thin-film silicon nitride and lithium niobate material system that uses segmented electrodes for RF and optical index matching is presented. The device uses a silicon handle and does not require substrate removal. A silicon handle allows the use of larger wafer sizes to increase yield, and lends itself to processing in established silicon foundries that may not have the capability to process a quartz or fused silica wafer. The modulator has an interaction region of 10 mm, shows a DC half wave voltage of 3.75 V, an ultra-high extinction ratio of roughly 45 dB consistent with previous work, and a fiber-to-fiber insertion loss of 7.47 dB with a 95 GHz 3 dB bandwidth.

© 2022 Optica Publishing Group

<http://dx.doi.org/10.1364/ao.XX.XXXXXX>

1. INTRODUCTION

Global networking traffic continues to grow past the capabilities of current infrastructure while existing systems become slow, inefficient and unreliable [1–4]. As coaxial transmission lines are upgraded to support the next communication standard and cellular towers reinforced to support their weight, a band-aid is applied to a deeper issue: existing hardware that supports these systems has reached the limit of its capabilities and must be replaced not only to maintain stable operation, but to raise the technological "ceiling" and pave the way for the faster, more reliable and more secure networks of the future. Fiber-optic cables can replace the heavy, lossy, and band-limited transmission lines of today's networks, but cannot be simply "plugged-in" to an existing antenna, networking hub, or cellular tower. We must introduce a "converter" that can read an RF signal meant

for a coaxial cable and convert it to an optical signal that can be transmitted through a fiber-optic cable. The optical modulator provides this capability [5]. Two approaches to optical modulation have risen to prominence in the last two decades: free-carrier dispersion-based modulation and electro-optic (EO) modulation [2, 5]. Free-carrier dispersion-based modulation involves the manipulation of free-carriers in a semiconductor to change the real and imaginary refractive index of the material, while electro-optic modulation takes advantage of the non-linear optical properties of a crystal to modulate a beam of light within an applied electric field [2, 6]. EO modulators show increased bandwidth, lower voltage operation, increased extinction ratio (ER), higher spurious-free dynamic range, zero chirping and increased power handling capability over their free-carrier dispersion counterparts [2, 4–8]. Thin-film lithium niobate (LiNbO₃) on insulator (TFLNOI) is chosen as the electro-optic medium for its high second-order non-linearity ($\chi^{(2)}$), low third-order non-linearity ($\chi^{(3)}$), low optical absorption, and exceptional environmental stability [2, 4, 6]. TFLNOI offers tighter mode confinement leading to a smaller footprint, and improved voltage-bandwidth performance over bulk LiNbO₃ devices [2, 8, 9]. To guide a tightly-confined optical mode and support the use of an on-chip fiber-coupler at the end facets of the device, silicon nitride (SiN_x) is chosen as the ideal candidate to form a low-loss strip-loaded waveguide on the TFLNOI [4, 7].

In previous work, co-planar waveguide (CPW) electrodes have been used to apply the RF modulating signal [4, 7, 8]. To closely match the RF phase and optical group index (n_{RF} and n_{og}), an index matching epoxy (Masterbond™ UV15) is applied to the interaction region between the signal and ground electrodes [4, 7]. However, the presence of the epoxy nearly doubles the RF loss (α_{RF}) over 100 GHz compared to a standard, unmatched CPW [4]. Moreover, it is not possible to precisely tune the RF index when using an index matching fluid, where a mismatch of even 1–2% between n_{og} and n_{RF} can greatly reduce the 3 dB bandwidth of the device [2, 6, 9]. Finally, UV15 is not environmentally stable, and may breakdown at high temperatures or in the presence of ultra-violet (UV) radiation. Micro-structured, or "segmented" electrodes have been used in literature to slow the RF phase velocity and match the RF and optical index [9–14]. This provides tunability of n_{RF} , and drastically reduces the RF loss compared to a UV15-clad electrode, increasing EO band-

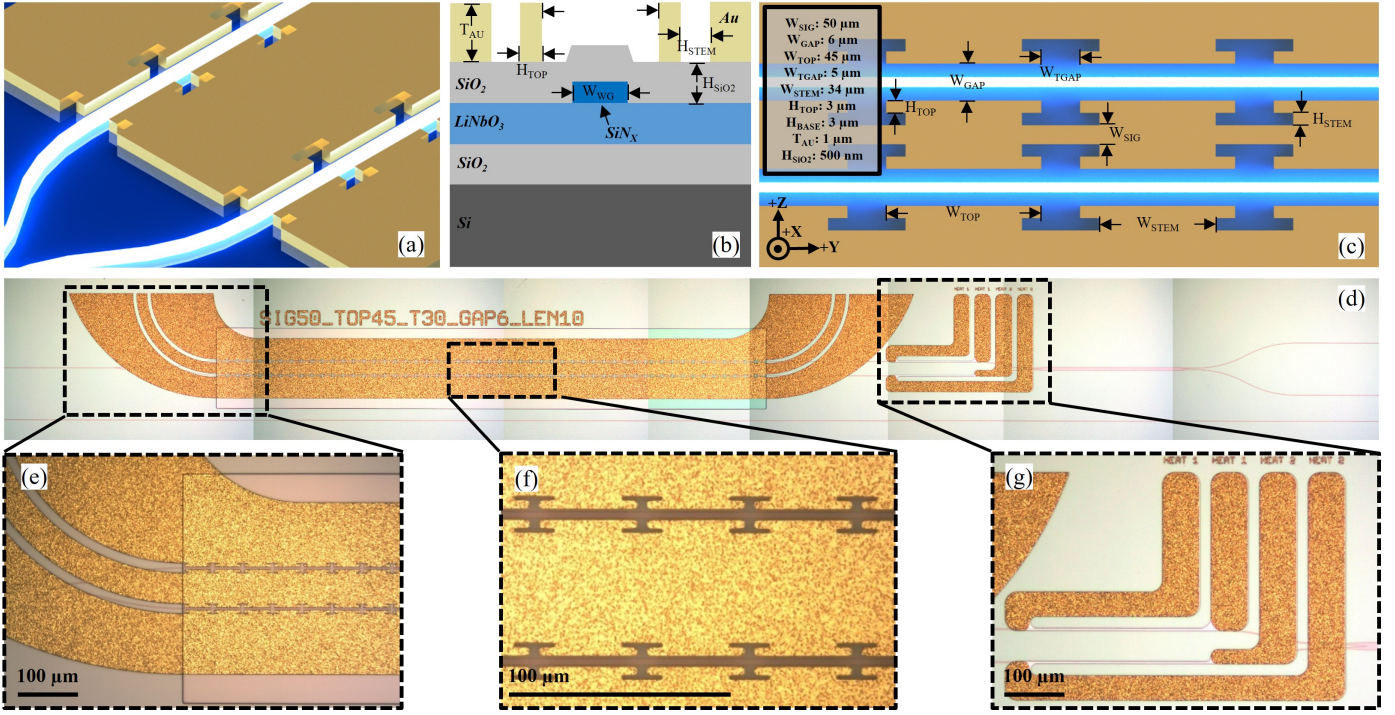


Fig. 1. (a) Artistic overview of the segmented electrode structures. (b) Cross-sectional view of the material stack and dimension definitions. (c) Top-down view of the segmented-electrodes with dimension definitions. (d) Top-down view of the fabricated device. Optical and RF propagation occurs from left to right. (e) Detail view of the transition from the probe-region to interaction region. (f) Detail view of the interaction region showing to-scale segmented electrodes. (g) Detail view of the thermal bias heaters.

width. However, these require either the use of a quartz handle or a complicated substrate-removal technique after electrode fabrication to match n_{og} and n_{RF} [9, 10]. These methods then preclude fabrication of the device in any established silicon foundry. In this work, a dual-output Mach Zehnder modulator (MZM) using micro-structured CPW electrodes is fabricated on a TFLNOI wafer with a silicon handle without the use of substrate removal or back-dicing techniques. An artist's rendition of the segmented electrodes is seen in Fig. 1. (a). A silicon handle allows the use of larger wafer sizes to increase yield and lends itself to processing in established silicon foundries that may not have the capability to process a quartz or fused silica wafer, or to etch through a LiNbO₃ layer. The modulator has an interaction region of 10 mm, shows a DC half wave voltage ($V\pi$) of 3.75 V, an ultra-high ER of roughly 45 dB, and a fiber-to-fiber insertion loss of 7.47 dB. The measured 3 dB bandwidth is roughly 95 GHz. To the best of our knowledge, this is the first time a traveling-wave EO modulator has been designed, fabricated and characterized with slow-wave segmented electrodes in the LiNbO₃ on Si material platform without substrate removal.

2. DESIGN AND FABRICATION

An optical modulator should maintain a small footprint and a wide RF bandwidth if it is to be used in the telecommunications system of the future [2, 5]. To achieve this, the traveling-wave EO modulator must have minimal RF loss and near-perfect index matching between n_{og} and n_{RF} [9]. The introduction of "T"-shaped segments along the interaction region of the electrode enables tuning of the RF phase velocity for better matching of n_{og} and n_{RF} through periodic capacitive loading, and can decrease current crowding within the electrode gap [9, 11–13]. Recently,

segmented electrodes have been designed and fabricated on quartz (Qz) and substrate-removed Si handles, and before that on III-V compound semi-conductor modulators to slow the RF traveling wave [9–11]. Here, we employ segmented electrodes on a Si handle without substrate removal to raise n_{RF} to 2.134 to match $n_{og} = 2.138$, where n_{RF} of a standard CPW in this material system is 1.92. Considering the relation between n_{RF} and the microwave impedance of the loaded line (Z_l) given by Eq. 1, we are able to tune the slowing of the wave by adjusting W_{STEM} to increase or decrease the inductance of the CPW by changing the effective distance that the current must travel along the electrode [11, 12].

$$Z_l = \sqrt{\frac{L_l}{C_l}}, \quad n_{RF} = c_0 \sqrt{L_l C_l} \quad (1)$$

Here, Z_l , L_l and C_l are the microwave impedance, inductance and capacitance of the loaded CPW, respectively, and c_0 is the speed of light. Considering the 500 nm height of the SiO₂ top cladding (T_{SiO2}) under the Au electrode, the electrode gap width (W_{GAP}) is set to 6 μm to avoid unwanted optical absorption loss from the optical mode interacting with the Au electrode. The voltage-length product ($V\pi \cdot L$) with different H_{CLAD} and W_{GAP} values is shown in Fig. 2. (a). These values can be adjusted to meet specific design goals [6, 15]. A lower $V\pi \cdot L$ can be achieved at the cost of RF and optical propagation loss when W_{GAP} and H_{CLAD} are made smaller, or by using a ridge-etched LiNbO₃ waveguide at the cost of excess coupling loss. The height of the top of the segment (H_{TOP}) is set to 3 μm, where RF loss may increase with a larger dimension. With $W_{TOP} = 45$ μm and $W_{TGAP} = 5$ μm to reduce the dispersion effect and raise the Bragg cutoff frequency above 1 THz, W_{STEM} is experimentally chosen to be 34 μm to achieve $n_{RF@120GHz} = 2.134$. Moreover, by varying

the width of W_{STEM} from 10 μm to 42 μm , and consequentially the inductance of the electrode, we were able to adjust the RF index from $n_{\text{RF}} = 2.3$ to $n_{\text{RF}} = 2.1$, proving the effectiveness of the design on different material systems. A comparison between measured L_l and C_l of the segmented and standard CPW is shown in Fig. 3. (f). Finally, H_{STEM} and W_{SIG} , and T_{AU} are set to 3 μm , 50 μm and 1 μm , respectively, to reduce RF loss and most closely match Z_l to the source impedance $Z_0 = 50 \Omega$. The effect of each dimension are shown in Table 1.

Table 1. Electrode Dimension vs. RF Index and Loss

Dimension	Size	RF Index (n_{RF})	RF Loss (α_{RF})
W_{SIG}	\uparrow	\uparrow	\downarrow
W_{GAP}	\uparrow	\downarrow	\downarrow
W_{TOP}	\uparrow	\uparrow	—
W_{TGAP}	\uparrow	—	—
W_{STEM}	\uparrow	\downarrow	\uparrow
H_{TOP}	\uparrow	\uparrow	\uparrow
H_{BASE}	\uparrow	\uparrow	\uparrow
T_{AU}	\uparrow	\downarrow	\downarrow

The Si handle has a relatively high permittivity ($\epsilon_{\text{Si}} = 11.7$) compared to Qz ($\epsilon_{\text{Qz}} = 4.5$), requiring W_{STEM} to be substantially wider than that of a segmented electrode fabricated on a Qz handle to maintain RF and optical index matching [16]. This allows more current to flow in the interaction region, and consequentially reduction in RF loss with segmented electrodes on an Si handle is not seen to the same extent as when using a Qz handle and a very narrow W_{STEM} [9, 11]. Regardless, the segmented electrodes reported in this manuscript eliminate the need for a UV15 cladding, which nearly doubles RF loss over 100 GHz [4, 7]. Through precise index matching, the EO modulator then shows a 3-dB EO bandwidth, over twice that of a UV15-clad device reported in previous work [4]. The aerial view of the EO modulator is shown in Fig. 1. (d), with high-resolution images of the probe-transition, interaction region and thermal bias heaters in Fig. 1. (e, f, g), respectively. Fabrication begins on a 300 nm X-cut TFLNOI slab procured from NanoLNTM. The material stack, from top to bottom is 500 nm of plasma-enhanced chemical vapor deposition (PECVD) SiO_2 , 100 nm of PECVD SiN_x , which defines the strip-loaded waveguide, 300 nm of X-cut LiNbO_3 , and 4.7 μm of thermal SiO_2 atop a 500 μm Si handle. All optical structures are defined with electron-beam lithography, while the electrodes are defined with a laser writer. The electrodes are 1 μm electroplated Au. The thickness and width of the SiN_x waveguide is 100 nm and 2 μm , respectively. With this, roughly 69 % of the optical mode is confined in the LiNbO_3 layer. The cross section of the waveguide and electrodes in the interaction region can be seen in Fig. 1. (b), a top-down view of the interaction region with dimensions labeled can be seen in Fig. 1. (c). The EO modulator employs a 1x2 MMI splitter at the beginning and a 2x2 MMI splitter/combiner at the end to produce two outputs with inversely-proportional optical intensities depending on the applied RF signal. Design, fabrication and characterization of these optical structures is discussed in previous work [4, 8].

3. RESULTS AND DISCUSSION

A Keysight PNA-X with range extenders and W-band ground-signal-ground probes is used to measure RF scattering parameters of the different electrode designs. In Fig. 3. (a), it is shown

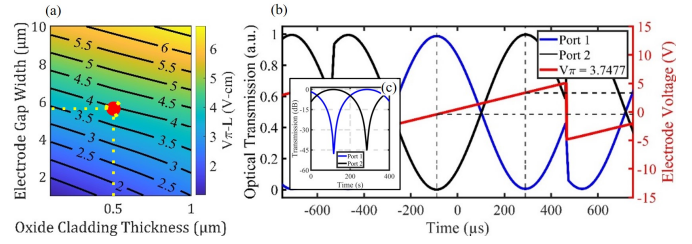


Fig. 2. (a) Heat-map comparing the effect of electrode W_{GAP} and T_{SiO_2} on $V\pi$ -L. (b) The measured DC- $V\pi$ of the device. The red trace shows applied electrode voltage, the blue and black traces show normalized optical intensity at output ports 1 and 2, respectively. (c) The measured ER of the device at both output ports.

that the UV15-cladding nearly doubles the RF loss of the electrode at 120 GHz where absorption loss in the UV15 becomes dominant. There is a rapid drop-off in $S(2,1)$ from DC to roughly 1 GHz from a low-frequency impedance mismatch. On the Si handle, with its high-microwave absorption tangent ($\tan\delta = 10^{-2}$), dielectric loss remains dominant over conductive or radiative losses [17]. Furthermore, considering $\epsilon_{\text{Si}} = 11.7$, W_{STEM} must be relatively wide to properly match n_{RF} and n_{og} which does not significantly reduce current bunching in the interaction region when compared to a standard CPW design [9]. As such, it is shown that there are no outstanding improvements to RF loss when compared outright to a standard CPW. Nevertheless, the RF loss is halved compared to an index-matched, UV15-clad CPW.

Z_l and n_{RF} are extracted from the measured scattering parameters and presented in Fig. 3. (b) and (c), respectively. While n_{RF} and n_{og} are extremely well matched at high frequencies, there is a ± 10 variation in Z_l along the frequency sweep. Considering the effect of Z_l on the AC- $V\pi$ and EO $S(2,1)$ penalty, following $(Z_l + 50\Omega)/2Z_l$ and $20\log(2Z_l/(Z_l + 50\Omega))$, respectively, a 10 Ω mismatch results in a 0.47 V increase in $V\pi$ and a 1 dB reduction in EO $S(2,1)$ [6, 9]. The DC EO response and ER of the device are presented in Fig. 2. (b) and (c), respectively. The DC $V\pi$ measures roughly 3.75 V, while the ER is >45 dB at each port. Both output ports show an output intensity inversely proportional to the other. The measured sideband power of the modulator from 1 GHz to 120 GHz is shown in Fig. 3. (d). Here, the device is operating at quadrature bias, and the sideband power is normalized to the carrier and RF input power. The measured 3-dB response of the modulator is roughly 95 GHz using 1 GHz as the reference frequency. A flattening of the sideband response can be seen above 70 GHz which corresponds to the gradual improvement in both Z_l and n_{RF} . This effect may be related to the total length of each segment, but has not been investigated [11]. The EO modulator shows a fiber-to-fiber insertion loss of roughly 7.47 dB using OZ Optics lensed fibers with a mode field diameter (MFD) of 2.5 μm . A reflectometer/light-wave analyzer is then used to determine the back-scatter and propagation loss in the device, shown in Fig. 3. (e). Optical propagation loss is roughly 0.69 dB/cm, which is consistent with previous work. The total length of the reference optical waveguide is roughly 30 mm which gives a total propagation loss of 2.07 dB, while an additional 2.7 dB of optical power is lost at each facet.

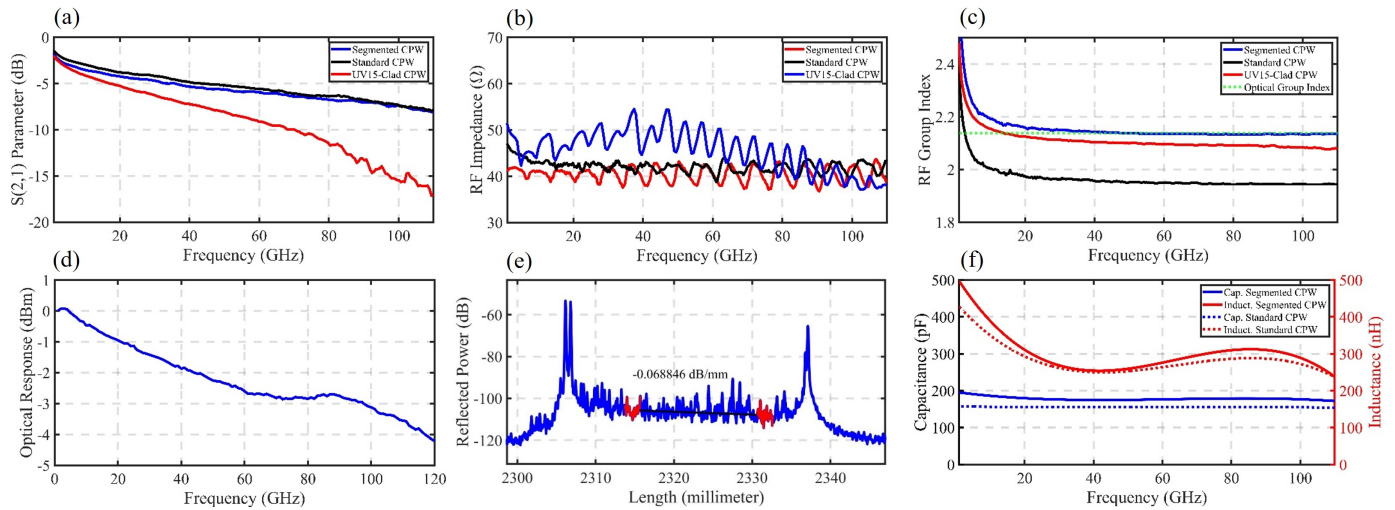


Fig. 3. (a) Measured $S(2,1)$ response of the CPW designs. (b) Measured impedance of the CPW designs. (c) Measured RF group index of the CPW designs. (d) Measured electro-optic response from 1-120 GHz. (e) Measured propagation loss and back-scat of the optical waveguide. (f) Capacitance and inductance of the CPW designs.

4. CONCLUSION

In this work, a high-speed, dual-output $\text{LiNbO}_3\text{-SiN}_x$ electro-optic MZM using segmented electrodes is fabricated on a Si handle without the need for substrate removal to demonstrate the feasibility of a micro-structured CPW in this material platform. Micro-structured electrodes provide tunability of n_{RF} , and drastically reduce the RF loss compared to a UV15-clad electrode, increasing EO bandwidth. The use of a Si handle allows the use of larger wafer sizes to increase yield in production environments, lends itself to processing in established Si foundries, and reduces the cost of upgrading existing systems with this new technology so that it may one day come to fruition in global telecommunications systems. Without the need for substrate removal or an index-matching epoxy, the device is extremely durable and can reliably operate in a myriad of environmental conditions. The modulator has an interaction region of 10 mm, shows a DC half wave voltage ($V\pi$) of 3.75 V, an ultra-high ER of over 45 dB at both output ports and a fiber-to-fiber insertion loss of 7.47 dB. The measured 3 dB bandwidth is roughly 95 GHz. Finally, there is a path forward for further improvement of RF performance by optimization of the "T"-structure to reduce current crowding in the interaction region.

5. BACKMATTER

Acknowledgments. This manuscript (AFRL-2022-2292) was supported in part under AFRL contract FA8650-19-C-1027. The authors gratefully acknowledge the support of UTA16-001296. The views and conclusions contained herein are those of the authors and should not be interpreted as necessarily representing the official policies or endorsements, either expressed or implied, of Air Force Research Laboratory, the Department of Defense, or the U.S. Government.

Disclosures. The authors declare no conflicts of interest.

Data Availability Statement. Data underlying the results presented in this paper are not publicly available at this time but may be obtained from the authors upon reasonable request.

6. REFERENCES

REFERENCES

1. A. Alvarado, D. J. Ives, S. J. Savory, and P. Bayvel, *J. Light. Technol.* **34**, 2339 (2016).
2. M. Zhang, C. Wang, P. Kharel, D. Zhu, and M. Lončar, *Optica* **8**, 652 (2021).
3. Y. Yue, Q. Wang, and J. Anderson, *Appl. Sci.* **9**, 2455 (2019).
4. S. Nelán, A. Mercante, C. Hurley, S. Shi, P. Yao, B. Shopp, and D. W. Prather, *Opt. Express* **30**, 9193 (2022).
5. E. Wooten, K. Kissa, A. Yi-Yan, E. Murphy, D. Lafaw, P. Hallemeier, D. Maack, D. Attanasio, D. Fritz, G. McBrien, and D. Bossi, *IEEE J. Sel. Top. Quantum Electron.* **6**, 69 (2000).
6. G. Ghione, *Semiconductor Devices for High-Speed Optoelectronics* (Cambridge University Press, 2009).
7. A. N. R. Ahmed, S. Shi, A. Mercante, S. Nelán, P. Yao, and D. W. Prather, *APL Photonics* **5**, 091302 (2020).
8. A. N. R. Ahmed, S. Nelán, S. Shi, P. Yao, A. Mercante, and D. W. Prather, *Opt. Lett.* **45**, 1112 (2020).
9. P. Kharel, C. Reimer, K. Luke, L. He, and M. Zhang, *Optica* **8**, 357 (2021).
10. G. Chen, K. Chen, R. Gan, Z. Ruan, Z. Wang, P. Huang, C. Lu, A. P. T. Lau, D. Dai, C. Guo, and L. Liu, *APL Photonics* **7**, 026103 (2022).
11. G. Li, T. Mason, and P. Yu, *J. Light. Technol.* **22**, 1789 (2004).
12. D. A. Motta, Y. R. R. Bustamante, A. P. Freitas, G. B. de Farias, U. C. Moura, and L. H. Gabrielli, "Design of a 40 GHz bandwidth slow-wave silicon modulator," in *2017 SBMO/IEEE MTT-S International Microwave and Optoelectronics Conference (IMOC)*, (IEEE, Aguas de Lindoia, 2017), pp. 1–5.
13. JaeHyuk Shin, S. R. Sakamoto, and N. Dagli, *J. Light. Technol.* **29**, 48 (2011).
14. X. Huang, Y. Liu, Z. Li, H. Guan, Q. Wei, Z. Yu, and Z. Li, *IEEE Photonics J.* **13**, 1 (2021).
15. J. A. Ibarra Fuste and M. C. Santos Blanco, *Opt. Lett.* **38**, 1548 (2013).
16. R.-Y. Yang, C.-Y. Hung, Y.-K. Su, M.-H. Weng, and H.-W. Wu, *Microw. Opt. Technol. Lett.* **48**, 1773 (2006).
17. N. Chudpooti, N. Duangrit, A. D. Burnett, J. R. Freeman, T. B. Gill, C. Phongcharoenpanich, U. Imberg, D. Torrungrueng, P. Akkaraekthalin, I. D. Robertson, and N. Somjit, *Mater. Res. Express* **8**, 056201 (2021).

FULL REFERENCES

1. A. Alvarado, D. J. Ives, S. J. Savory, and P. Bayvel, "On the Impact of Optimal Modulation and FEC Overhead on Future Optical Networks," *J. Light. Technol.* **34**, 2339–2352 (2016).
2. M. Zhang, C. Wang, P. Kharel, D. Zhu, and M. Lončar, "Integrated lithium niobate electro-optic modulators: when performance meets scalability," *Optica* **8**, 652 (2021).
3. Y. Yue, Q. Wang, and J. Anderson, "Experimental Investigation of 400 Gb/s Data Center Interconnect Using Unamplified High-Baud-Rate and High-Order QAM Single-Carrier Signal," *Appl. Sci.* **9**, 2455 (2019).
4. S. Nelan, A. Mercante, C. Hurley, S. Shi, P. Yao, B. Shopp, and D. W. Prather, "Compact thin film lithium niobate folded intensity modulator using a waveguide crossing," *Opt. Express* **30**, 9193 (2022).
5. E. Wooten, K. Kissa, A. Yi-Yan, E. Murphy, D. Lafaw, P. Hallemeier, D. Maack, D. Attanasio, D. Fritz, G. McBrien, and D. Bossi, "A review of lithium niobate modulators for fiber-optic communications systems," *IEEE J. Sel. Top. Quantum Electron.* **6**, 69–82 (2000).
6. G. Ghione, *Semiconductor Devices for High-Speed Optoelectronics* (Cambridge University Press, 2009).
7. A. N. R. Ahmed, S. Shi, A. Mercante, S. Nelan, P. Yao, and D. W. Prather, "High-efficiency lithium niobate modulator for K band operation," *APL Photonics* **5**, 091302 (2020).
8. A. N. R. Ahmed, S. Nelan, S. Shi, P. Yao, A. Mercante, and D. W. Prather, "Subvolt electro-optical modulator on thin-film lithium niobate and silicon nitride hybrid platform," *Opt. Lett.* **45**, 1112 (2020).
9. P. Kharel, C. Reimer, K. Luke, L. He, and M. Zhang, "Breaking voltage–bandwidth limits in integrated lithium niobate modulators using micro-structured electrodes," *Optica* **8**, 357 (2021).
10. G. Chen, K. Chen, R. Gan, Z. Ruan, Z. Wang, P. Huang, C. Lu, A. P. T. Lau, D. Dai, C. Guo, and L. Liu, "High performance thin-film lithium niobate modulator on a silicon substrate using periodic capacitively loaded traveling-wave electrode," *APL Photonics* **7**, 026103 (2022).
11. G. Li, T. Mason, and P. Yu, "Analysis of Segmented Traveling-Wave Optical Modulators," *J. Light. Technol.* **22**, 1789–1796 (2004).
12. D. A. Motta, Y. R. R. Bustamante, A. P. Freitas, G. B. de Farias, U. C. Moura, and L. H. Gabrielli, "Design of a 40 GHz bandwidth slow-wave silicon modulator," in *2017 SBMO/IEEE MTT-S International Microwave and Optoelectronics Conference (IMOC)*, (IEEE, Aguas de Lindoia, 2017), pp. 1–5.
13. JaeHyuk Shin, S. R. Sakamoto, and N. Dagli, "Conductor Loss of Capacitively Loaded Slow Wave Electrodes for High-Speed Photonic Devices," *J. Light. Technol.* **29**, 48–52 (2011).
14. X. Huang, Y. Liu, Z. Li, H. Guan, Q. Wei, Z. Yu, and Z. Li, "Advanced Electrode Design for Low-Voltage High-Speed Thin-Film Lithium Niobate Modulators," *IEEE Photonics J.* **13**, 1–9 (2021).
15. J. A. Ibarra Fuste and M. C. Santos Blanco, "Bandwidth–length trade-off figures of merit for electro-optic traveling wave modulators," *Opt. Lett.* **38**, 1548 (2013).
16. R.-Y. Yang, C.-Y. Hung, Y.-K. Su, M.-H. Weng, and H.-W. Wu, "Loss characteristics of silicon substrate with different resistivities," *Microw. Opt. Technol. Lett.* **48**, 1773–1776 (2006).
17. N. Chudpooti, N. Duangrit, A. D. Burnett, J. R. Freeman, T. B. Gill, C. Phongcharoenpanich, U. Imberg, D. Torrungrueng, P. Akkaraekthalin, I. D. Robertson, and N. Somjit, "Wideband dielectric properties of silicon and glass substrates for terahertz integrated circuits and microsystems," *Mater. Res. Express* **8**, 056201 (2021).